2021 43rd Annual International Conference of the
IEEE Engineering in Medicine & Biology Society (EMBC)
Oct 31 - Nov 4, 2021. Virtual Conference

Reconstruction of stomach geometry using magnetic source localization

Chad E. Eichler, Leo K. Cheng, Niranchan Paskaranandavadivel, Saeed Alighaleh,
Timothy R. Angeli-Gordon, Peng Du, Leonard A. Bradshaw, and Recep Avci

Abstract— **Routine diagnosis of gastric motility disorders represents a significant problem to current clinical practice. The non-invasive electrogastrogram (EGG) and magnetogastrogram (MGG) enable the assessment of gastric slow wave (SW) dysrhythmias that are associated with motility disorders. However, both modalities lack standardized methods for reliably detecting patterns of SW activity. Subject-specific anatomical information relating to the geometry of the stomach and its position within the torso have the potential to aid the development of relations between SWs and far-fields. In this study, we demonstrated the feasibility of using magnetic source localization to reconstruct the geometry of an anatomically realistic 3D stomach model. The magnetic fields produced by a small (6.35×6.35 mm) N35 neodymium magnet sequentially positioned at 64 positions were recorded by an array of 27 magnetometers. Finally, the magnetic dipole approximation and a particle swarm optimizer were used to estimate the position and orientation of the permanent magnet. Median position and orientation errors of 3.8 mm and 7.3° were achieved. The estimated positions were used to construct a surface mesh, and the Hausdorff Distance and Average Hausdorff Distance dissimilarity metrics for the reconstructed and ground-truth models were 11.6 mm and 2.4 mm, respectively. The results indicate that source localization using the magnetic dipole model can successfully reconstruct the geometry of the stomach.**

Clinical relevance—**Concurrent recordings of stomach geometry and slow wave activity can provide insights into how non-invasive far-field measurements relate to the underlying activity and can enhance the non-invasive detection of dysrhythmias.**

I. Introduction

Rhythmic electrical activity known as slow waves (SWs) are, in part, responsible for the muscular contractions that enable gastrointestinal (GI) motility. High resolution serosal mapping of SW activity is the state-of-the-art method for recording SW activation and propagation, however, its invasiveness limits its utility as a routine diagnostic tool [1], [2], [3]. Electrical potentials and magnetic fields (MFs) generated by SW activity can also be recorded non-invasively in the form of the electrogastrogram (EGG) using cutaneous electrodes and the magnetogastrogram (MGG) using superconducting quantum interference devices (SQUIDs) [4]. Both of these modalities have demonstrated the ability to assess spatio-temporal characteristics of SWs, but they both suffer from several limitations such as difficulties in recording, signal processing, and correlations with SW activation and propagation patterns [5], [6]. Consequently, the adoption of EGG and MGG has been limited to a limited number of specialized research institutions.

Concurrent far-field and serosal or mucosal recordings have been used to develop relations between far-field signals and the underlying SW activity, however, the relative position and geometry of the stomach and the recording arrays were not quantitatively recorded in these studies [5], [7]. The accurate registration of far-fields, serosal activity, and subject anatomy in a global coordinate system could aid the development of far-field analysis techniques by enhancing correlations.

Imaging modalities such as computer tomography (CT) or magnetic resonance imaging (MRI) are typically used to reconstruct the stomach geometry. Performing EGG and HR mapping concurrently with either CT or MRI imaging is challenging and the limitations of MGG prohibit concurrent imaging altogether. The concurrent recording of anatomical information is important because the position and conformation of the stomach can change due to digestion, body position, and weight changes. Furthermore, it is essential to record the relative position of the electrodes and far-field sensors at the time that SW recordings are made. Therefore, there is a need for a novel and robust method to extract geometric information in surgical settings.

Magnetic tracking systems have been used to monitor the position of medical devices or anatomical structures within the human body when visibility is impaired [8], [9], [10]. High localization accuracy can be achieved using this approach because the human body is highly permeable to MFs [8]. In this study, the feasibility and performance of using magnetic source localization to reconstruct the 3D geometry of the stomach was investigated.

II. Methods

A. Magnetic Field Recording System

A MF recording system with 27 magnetometers was developed. The 3-axis HMC1053 magnetometer (Honeywell, Charlotte, NC, USA) was used because of its small size ($7.37 \times 7.37 \times 2.79$ mm), low noise density (50 nV$\cdot$ Hz^2), wide sensing range (± 0.6 mT), and Set/Reset strap. A circuit was constructed to amplify (gain = 100), and low-pass filter (cutoff = 3 Hz) the sensor output signals, and to transmit the filtered signals to an ActiveTwo data-acquisition system (BioSemi, Amsterdam, Netherlands) operating at a sampling frequency of 2048 Hz. The ActiveTwo unit was modified for passive recording. The circuit also applied a 2–4 A current

*Research supported by Health Research Council of New Zealand, the Marsden Fund Council of New Zealand, and NIH (R01 HD 088662).

C. E. Eichler, L. K. Cheng, N. Paskaranandavadivel, S. Alighaleh, T. R. Angeli-Gordon, P. Du, and R. Avci are with the Auckland Bioengineering Institute, University of Auckland, Auckland, New Zealand. E-mail: recep.avci@auckland.ac.nz

L. K. Cheng and L. A. Bradshaw are with the Department of Surgery, Vanderbilt University, Nashville, TN, USA

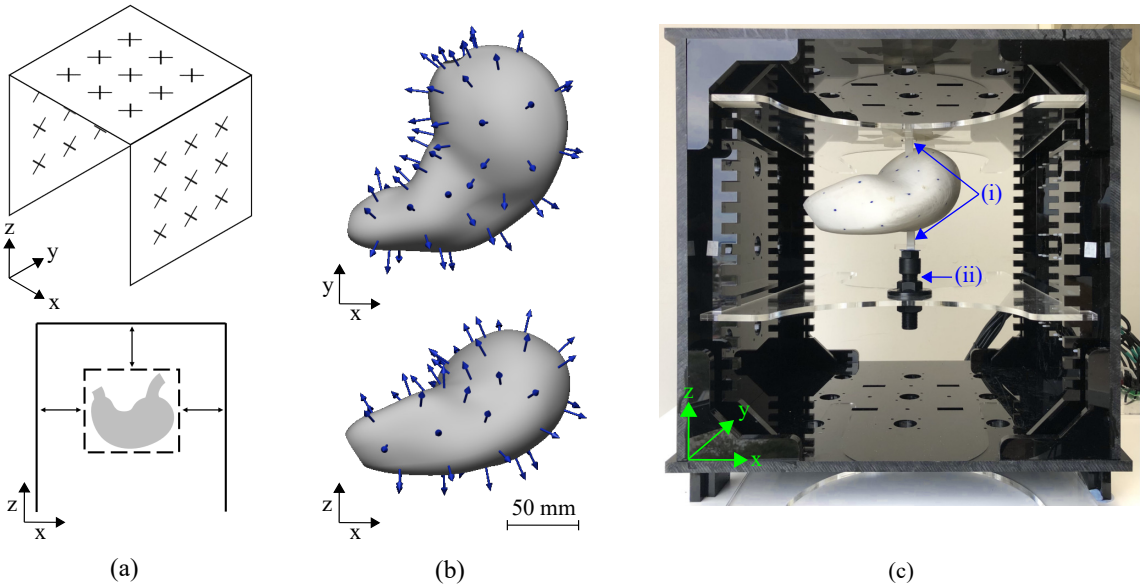

Fig. 1. Sensor array schematic and mounting protocol for the stomach model. (a) Two views of the sensory array schematic are shown. The sensor array consists of 3 planes each with an evenly spaced 3 × 3 grid of sensors. (b) The top and side views of the anatomically realistic stomach geometry are presented. The nodes to be localized are represented by blue arrows which are oriented perpendicular to the stomach surface. These nodes were marked in the geometry so that they were present in the 3D-printed model. (c) A photograph of the 3D-printed model clamped within the array is shown. The model has two vertical support rods (i). A threaded clamp pin (ii) secures the model against the center of an acrylic panel that is positioned at a known height. The known height of this panel enables the coordinate system of the model to be registered to that of the sensor array. Furthermore, the nodes for localization on the 3D-printed model are colored blue.

pulse (2 μs pulse-width at 20 Hz) to the Set/Reset strap of the magnetometer to maintain a high sensitivity state.

The sensor array consisted of 3 planes of 9 sensors positioned in an upside-down "U" formation which could easily be positioned over a subject during a surgical operation (Fig. 1(a)). Each sensor plane was 400 × 400 mm and was composed of a 3 × 3 grid of sensors spaced evenly at intervals of 100 mm (center-to-center).

B. Experimental Design

The MF recording system and geometry reconstruction via source localization was validated using a 3D-printed stomach model where a cylindrical N35 Grade Neodymium (Nd-Fe-B) magnet 6.35 mm in diameter and 6.35 mm in length was used as the magnetic source. The magnetic moment constant for this magnet was determined through calibration.

A series of nodes with known locations were labelled on a pre-existing anatomically realistic stomach geometry [11] such that they could be identified when the model was 3D-printed. The node locations were chosen by first placing 8 evenly spaced paths from the esophageal sphincter to the pyloric sphincter on the stomach surface. Then, 8 nodes were positioned along each of these paths such that there were 64 nodes in total (Fig. 1(b)). Finally, a 1:1 scale 3D model of this geometry with the 64 labelled node positions was printed (MakerBot, New York, NY, USA).

The 3D-printed model was secured within the sensor array, and the coordinate system of the stomach model was registered to the coordinate system of the sensor array by clamping it at a known location using support rods (Fig. 1(c)). The MFs at all sensors were then recorded when the magnet was secured to the surface of the stomach at each of the 64 nodes. The same pole of the magnet was secured against the surface of the stomach at each node so that the accuracy of solving for source orientation could also be assessed. A moving average filter with a window width of 1 s was then applied to the data.

C. Source Localization

The magnetic dipole (MDP) model [8] was used for source localization and is defined as:

$$\mathbf{b}(\mathbf{d}, \mathbf{H_0}) = \frac{\mu_r \mu_0 M}{4\pi} \left(\frac{3\hat{\mathbf{d}} \left(\mathbf{H}_0 \cdot \hat{\mathbf{d}} \right) - \mathbf{H}_0}{\|\mathbf{d}\|^3} \right) \quad (1)$$

where $\mathbf{b}$ is the magnetic flux density, $\mathbf{d} = r_s - r_o$ is a vector from the sensor $\mathbf{r}_o$ to the center of the source $\mathbf{r}_s$, $\mathbf{H}_0$ is a vector that describes the orientation of the dipole, μ_r is the relative permeability of the medium, μ_0 is the magnetic permeability of free space, M is the magnetic moment constant, $\hat{\mathbf{d}}$ is a unit vector, and $\|\cdot\|$ is the Euclidean norm.

A cost function C was defined to quantify the difference between the measured and computed MFs for all n sensors:

$$C = \sum_{i=1}^{n} \|\mathbf{b}_{m,i} - \mathbf{b}_{f,i}\|^2 \quad (2)$$

where $\mathbf{b}_{m,i}$ and $\mathbf{b}_{f,i}$ are the measured and forward computed MFs at the i^{th} sensor. The position $\mathbf{r}_s$ and orientation

$\mathbf{H}_0$ of the source were then estimated by minimizing the cost function using the implementation of particle swarm optimization in MATLAB R2020a (MathWorks Inc, Natick, MA, USA) [12].

D. Geometry Reconstruction and Evaluation

The estimated source position was translated towards the stomach surface along the estimated dipole orientation by half of the 6.35 mm length of the magnet. This was done so that the estimated positions would theoretically lie on the stomach surface rather than at the center of the magnet.

Source localization performance was quantified using point-to-point Euclidean error and orientation error. Euclidean error was computed from the estimated $\mathbf{r}_s^*$ and ground-truth $\mathbf{r}_s$ node positions for the j^{th} node:

$$\epsilon_j = \|\mathbf{r}_{s,j}^* - \mathbf{r}_{s,j}\| \tag{3}$$

Orientation error was computed from the estimated $\mathbf{H}_0^*$ and ground-truth $\mathbf{H}_0$ normal vectors for the j^{th} node:

$$\theta = acos(\hat{\mathbf{H}}_{0,j}^* \cdot \hat{\mathbf{H}}_{0,j}) \tag{4}$$

A triangular surface mesh was then constructed from the estimated node positions and refined producing a surface mesh with 32,256 vertices. The accuracy of the reconstructed surface mesh was then compared against the ground-truth stomach geometry which was defined by 73,984 vertices. The Hausdorff Distance (HD) and the Average Hausdorff Distance (AHD) dissimilarity metrics were used in comparison and HD was computed from [13]:

$$HD(A,B) = \max\left(h(A,B), h(B,A)\right) \tag{5}$$

where A and B are the sets of vertices in the reconstructed and ground-truth geometries, respectively, and h(A,B) is given by:

$$h(A,B) = \max_{a\in A} \min_{b\in B} \|a-b\| \tag{6}$$

Similarly, AHD was computed from [13]:

$$AHD(A,B) = \max\left(k(A,B), k(B,A)\right) \tag{7}$$

where k(A,B) is given by:

$$k(A,B) = \frac{1}{N}\sum_{a\in A} \min_{b\in B} \|a-b\| \tag{8}$$

III. Results

The separation between the nodes and the closest sensor plane ranged between 86 mm and 191 mm (Fig. 1(c)). The median Euclidean error for the localized nodes was 3.8 mm, and the lower and upper quartiles were 3.0 mm and 5.6 mm, respectively (Fig. 2(a)). Additionally, the maximum Euclidean error was 11.3 mm. As shown in Fig. 3(a), Euclidean error was relatively uniformly distributed along the stomach, although the node with the largest error was located on the underside of the stomach and the separation between this node and the closest sensor plane was relatively large.

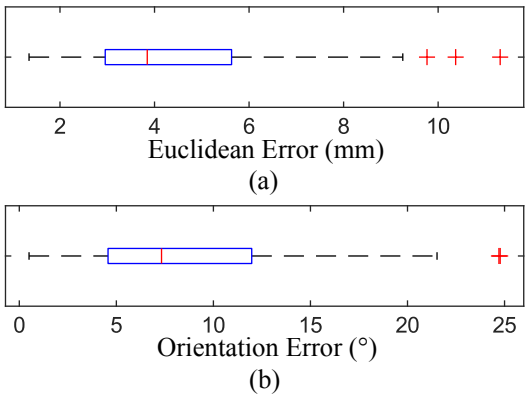

Fig. 2. Magnet localization errors. Euclidean position error is presented in (a) and the orientation error is presented in (b).

The median orientation error for the localized nodes was 7.3°, and the lower and upper quartiles were 4.6° and 12.0°, respectively (Fig. 2(b)). Notably, there was an outlier present at 24.7°. Similar to Euclidean position error, orientation error was also uniformly distributed throughout the stomach.

The triangular mesh constructed from the localized node positions is displayed in Fig. 3(b), where it is also compared against the ground-truth stomach geometry. This figure indicates that the dominant geometric features of the two models are consistent. Furthermore, the AHD and HD metrics were 2.4 mm and 11.6 mm, respectively.

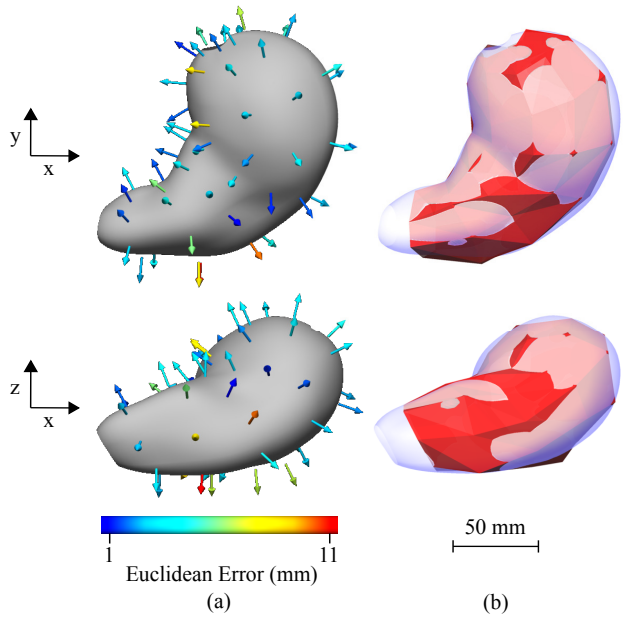

Fig. 3. Stomach geometry reconstruction results. The magnet localization position and orientation results are shown in (a) as arrows, where arrow color represents Euclidean position error. A comparison between the triangular surface mesh constructed from the localized nodes and the ground-truth model is presented in (b), where the models are colored red and transparent blue, respectively.

IV. Discussion

In this study, the feasibility and performance of using magnetic source localization to reconstruct the 3D geometry of the stomach was investigated. First, the MFs generated by a magnet at 64 known locations on the surface of a 3D-printed stomach model were recorded. The position and orientation of the magnet were then estimated using magnetic source localization and used to construct a triangular mesh. The accuracy of the localized nodes and the reconstructed stomach model was then assessed.

The median Euclidean error of 3.8 mm suggests that the accuracy of the localization system is sufficient for reconstruction of the stomach geometry as this error is relatively small compared to total size of the model. From visual inspection, the triangular mesh constructed from the localized nodes was able to approximate the bulk curvature of the stomach geometry (Fig. 3(c)). In the future, the accuracy of the reconstruction could be increased through repeated measurement or the use of a smoothing function. Due to the ability of magnetic source localization to resolve source orientation, it would also be possible to use the estimated surface-normal vectors as constraints at each node to improve the reconstruction. The median orientation error of 7.3° suggests that the accuracy of the estimated surface-normal vectors would be sufficient for this purpose.

The AHD error for the reconstruction was higher than what can be achieved using alternative reconstruction methods such as CT and MRI imaging, which can both reach accuracies as low as approximately 0.6 mm (RMS) [14]. However, there are significant challenges in performing either CT or MRI imaging concurrently with far-field modalities. Our results have shown that magnetic source localization is a promising alternative for stomach geometry reconstruction that can be performed concurrently with EGG and MGG.

Sophisticated analysis techniques for the far-fields generated by SWs are needed because many SW dysrythmias are spatially complex and do not produce signals at distinct frequencies [15]. The ability to reconstruct the stomach geometry at the time that far-field measurements are recorded has the potential to aid the development of far-field based source characterization techniques. As the geometry and position of the stomach within the torso has a large impact on how SWs appear as far-fields, this anatomical information could enhance correlations and lead to signatures for certain patterns of activity. Furthermore, this anatomical information could benefit modelling studies by facilitating validation.

Although the invasive nature of placing magnetic sources on the serosal surface of the stomach would prohibit clinical applications, this approach is intended to augment on-going animal studies. However, these methods could potentially be translated to an endoscopic approach used in combination with mucosal electrical mapping [16]. This would provide a more practical option for translating this work to clinical and chronic animal research studies. In addition, in vivo studies are necessary to validate the proposed method of stomach geometry reconstruction. The magnetic noise level in experimental settings may reduce reconstruction accuracy, however, the generation of alternating instead of static MFs would enable this interference to be mitigated. Additionally, the attenuation of the MFs by body tissues may also decrease reconstruction accuracy.

Further work to improve the recording system could involve replacing the magnet with an array of electromagnetic coils, as previously demonstrated in an in silico investigation [17]. This would enable the on-demand generation of more complex MFs and eliminate the need to manually reposition the source.

References

[1] P. Du, *et al.*, "High-resolution Mapping of In Vivo Gastrointestinal Slow Wave Activity Using Flexible Printed Circuit Board Electrodes: Methodology and Validation," *Ann. Biomed. Eng.*, vol. 37, no. 4, pp. 839–846, 2009.

[2] G. O'Grady, *et al.*, "Methods for high-resolution electrical mapping in the gastrointestinal tract," *IEEE Rev. Biomed. Eng.*, vol. 12, pp. 287–302, 2018.

[3] T. R. Angeli, *et al.*, "Loss of Interstitial Cells of Cajal and Patterns of Gastric Dysrhythmia in Patients With Chronic Unexplained Nausea and Vomiting," *Gastroenterology*, vol. 149, no. 1, pp. 56–66, 2015.

[4] R. Avci, *et al.*, "Bioelectrical Signals for the Diagnosis and Therapy of Functional Gastrointestinal Disorders," *Appl. Sci.*, vol. 10, no. 22, p. 8102, 2020.

[5] L. A. Bradshaw, J. H. Kim, S. Somarajan, W. O. Richards, and L. K. Cheng, "Characterization of electrophysiological propagation by multichannel sensors," *IEEE Trans. Biomed. Eng.*, vol. 63, no. 8, pp. 1751–1759, 2016.

[6] A. A. Gharibans, S. Kim, D. C. Kunkel, and T. P. Coleman, "High-Resolution Electrogastrogram: A Novel, Noninvasive Method for Determining Gastric Slow-Wave Direction and Speed," *IEEE Trans. Biomed. Eng.*, vol. 64, no. 4, pp. 807–815, 2017.

[7] S. Somarajan, *et al.*, "Noninvasive Magnetogastrography Detects Erythromycin-Induced Effects on the Gastric Slow Wave," *IEEE Trans. Biomed. Eng.*, vol. 66, no. 2, pp. 327–334, 2019.

[8] Z. Sun, *et al.*, "A Non-invasive Real-time Localization System for Enhanced Efficacy in Nasogastric Intubation," *Ann. Biomed. Eng.*, vol. 43, no. 12, pp. 2941–2952, 2015.

[9] H. Mateen, R. Basar, A. U. Ahmed, and M. Y. Ahmad, "Localization of Wireless Capsule Endoscope: A Systematic Review," *IEEE Sens. J.*, vol. 17, no. 5, pp. 1197–1206, 2017.

[10] C. Cheng, X. Huo, and M. Ghovanloo, "Towards a magnetic localization system for 3-D tracking of tongue movements in speech-language therapy," *Proc. Annu. Int. Conf. IEEE Eng. Med. Biol. Soc. EMBS*, vol. 176, no. 5, pp. 563–566, 2009.

[11] C. E. Eichler, *et al.*, "Effects of magnetogastrography sensor configurations in tracking slow wave propagation," *Comput. Biol. Med.*, vol. 129, p. 104169, 2021.

[12] R. Poli, J. Kennedy, and T. Blackwell, "Particle swarm optimization," *Swarm Intell.*, vol. 1, no. 1, pp. 33–57, 2007.

[13] A. A. Taha and A. Hanbury, "Metrics for evaluating 3D medical image segmentation: Analysis, selection, and tool," *BMC Med. Imaging*, vol. 15, no. 1, 2015.

[14] J. Van den Broeck, E. Vereecke, R. Wirix-Speetjens, and J. Vander Sloten, "Segmentation accuracy of long bones," *Med. Eng. Phys.*, vol. 36, no. 7, pp. 949–953, 2014.

[15] G. O'Grady, *et al.*, "Recent progress in gastric arrhythmia: Pathophysiology, clinical significance and future horizons," *Clin. Exp. Pharmacol. Physiol.*, vol. 41, no. 10, pp. 854–862, 2014.

[16] T. R. Angeli, *et al.*, "High-resolution electrical mapping of porcine gastric slow-wave propagation from the mucosal surface," *Neurogastroenterol. Motil.*, vol. 29, no. 5, 2017.

[17] R. Avci, *et al.*, "Computational Reconstruction of 3D Stomach Geometry using Magnetic Field Source Localization," *Proc. Annu. Int. Conf. IEEE Eng. Med. Biol. Soc. EMBS*, vol. 2020-July, pp. 2376–2379, 2020.